doi:10.1016/j.jmb.2010.04.021 J. Mol. Biol. (2010) 399, 464–475

JMB

Available online at www.sciencedirect.com

ScienceDirect

ELSEVIER

Structure of the Mitochondrial Editosome-Like Complex Associated TUTase 1 Reveals Divergent Mechanisms of UTP Selection and Domain Organization

Jason Stagno[1,2], Inna Aphasizheva[3], Jessica Bruystens[1,2], Hartmut Luecke[1,2,4,5]* and Ruslan Aphasizhev[3]*

[1]*Department of Molecular Biology and Biochemistry, University of California, Irvine, CA 92697, USA*

[2]*Center for Biomembrane Systems, University of California, Irvine, CA 92697, USA*

[3]*Department of Microbiology and Molecular Genetics, School of Medicine, University of California, Irvine, CA 92697, USA*

[4]*Department of Physiology and Biophysics, University of California, Irvine, CA 92697, USA*

[5]*Department of Information and Computer Sciences, University of California, Irvine, CA 92697, USA*

Received 19 January 2010; received in revised form 10 April 2010; accepted 13 April 2010
Available online 18 April 2010

Edited by I. Wilson

RNA uridylylation reactions catalyzed by terminal uridylyl transferases (TUTases) play critical roles in the formation of the mitochondrial transcriptome in trypanosomes. Two mitochondrial RNA editing TUTases have been described: RNA editing TUTase 1 catalyzes guide RNA, ribosomal RNA, and mRNA 3′-uridylylation, and RNA editing TUTase 2 acts as a subunit of the RNA editing core complex (also referred to as the 20S editosome) to perform guided U-insertion mRNA editing. Although RNA editing TUTase 1 and RNA editing TUTase 2 carry out distinct functions and possess dissimilar enzymatic properties, their catalytic N-terminal domain and base recognition C-terminal domain display a high degree of similarity, while their middle domains are less conserved. MEAT1 (*m*itochondrial *e*ditosome-like complex *a*ssociated *T*UTase 1), which interacts with an editosome-like assembly and is exclusively U-specific, nonetheless shows limited similarity with editing TUTases and lacks the middle domain. The crystal structures of apo MEAT1 and UTP-bound MEAT1 refined to 1.56 Å and 1.95 Å, respectively, reveal an unusual mechanism of UTP selection and domain organization previously unseen in TUTases. In addition to established invariant UTP-binding determinants, we have identified and verified critical contributions of MEAT1-specific residues using mutagenesis. Furthermore, MEAT1 possesses a novel bridging domain, which extends from the C-terminal domain and makes hydrophobic contacts with the N-terminal domain, thereby creating a cavity adjacent to the UTP-binding site. Unlike the minimal TUT4 TUTase, MEAT1 shows no appreciable conformational change upon UTP binding and apparently does not require RNA substrate to select a cognate nucleoside triphosphate. Because MEAT1 is essential for the viability of the bloodstream and insect forms of *Trypanosoma brucei*, the unique organization of its active site renders this protein an attractive target for trypanocide development.

Keywords: Trypanosoma; mitochondria; RNA editing; TUTase

**Corresponding authors.* E-mail addresses: hudel@uci.edu; ruslan@uci.edu.

Present addresses: J. Stagno, Center for Cancer Research, National Cancer Institute, National Institutes of Health, Frederick, MD 21702, USA; J. Bruystens, Department of Chemistry and Biochemistry, University of California, San Diego, La Jolla, CA 92093, USA.

Abbreviations used: TUTase, terminal uridylyl transferase; ncPAP, noncanonical Trf4/5-type poly(A) polymerase; RET1, RNA editing TUTase 1; RET2, RNA editing TUTase 2; NTD, N-terminal domain; CTD, C-terminal domain; BD, bridging domain; Pol β, DNA polymerase β like.

Introduction

Terminal uridylyl transferases (TUTases) are functionally and structurally diverse enzymes that catalyze template-independent 3′-uridylylation of single-stranded RNAs and guide-RNA-dependent internal U-insertions. Within the DNA polymerase β-type superfamily, TUTases are most closely related to noncanonical Trf4/5-type poly(A) polymerases (ncPAPs). It seems possible that the lack of transcriptional control for trypanosomal nuclear and mitochondrial genomes is partially compensated for by a diversity of TUTases and ncPAPs.[1] To that end, two nuclear ncPAPs (ncPAP1 and ncPAP2),[2] two mitochondrial poly(A) polymerases (KPAP1 and KPAP2),[3,4] two cytoplasmic TUTases (TUT3 and TUT4),[5,6] and three mitochondrial TUTases [RNA editing TUTase 1 (RET1), RNA editing TUTase 2 (RET2), and MEAT1 (*m*itochondrial *e*ditosome-like complex *a*ssociated *T*UTase 1)][7–9] have been identified in *Trypanosoma brucei*. Presently, functional data are available only for mitochondrial TUTases.

Mitochondrial DNA of kinetoplastid protozoans represents a catenated network composed of a few maxicircles and thousands of minicircles. Both strands of the maxicircles' conserved region are transcribed as polycistronic RNAs that are then cleaved into ribosomal RNA and mRNA precursors. Uridylylation catalyzed by the founding member of the TUTase family, RET1, takes place at the 3′-end of all known classes of mitochondrial RNAs. Ribosomal RNAs and guide RNAs receive ~20-nt-long U-tails, while most mRNAs bear long (A/U) heteropolymers synthesized by the concerted actions of RET1 and the mitochondrial poly(A) polymerase KPAP1.[10] RET2 exists as a subunit of the RNA editing core complex (also referred to as the 20S editosome)[11] and is responsible for U-insertion mRNA editing activity.[12,13] A high degree of sequence similarity between the catalytic N-terminal domain (NTD) and the C-terminal domain (CTD) in RET1 and RET2 indicates general conservation of these modules, but provides little cues for the differences in quaternary structure, UTP specificity, processivity, and functional interactions.

Crystallographic studies of *Tb*RET2[14] and cytosolic *Tb*TUT4[6,15] revealed a domain organization previously unseen among nucleotidyl transferases: the NTD and the CTD share a large interface, essentially creating a spherically shaped bidomain. The anti-parallel β-sheet of the NTD and two helices in the CTD form a deep cleft, which harbors three catalytic aspartates and a UTP-binding site. The distribution of critical active-center residues between the NTD and the CTD revealed a clear functional distinction between these two domains. The highly conserved NTD bears three universal metal-binding carboxylates and residues interacting with the triphosphate moiety, a common feature of all NTPs. The specificity for UTP substrate comes from nucleotide base interactions with the CTD.[6,14] In RET2, an additional middle domain is inserted between two β-strands at the C-terminus of the NTD. Remarkably, in RET1 and RET2, the middle domains are inserted at a highly conserved position, while their primary structures are dissimilar. In RET2, the middle domain extends into the solvent while maintaining extensive interactions with the CTD; its positioning and surface charge are consistent with a potential role in RNA binding.[14] Indeed, deletion of the middle domain in either RET1[16] or RET2[17] led to enzyme inactivation, indicating its essential function.

Discovery of a third mitochondrial TUTase, MEAT1, added more complexity to structure–function relationships among trypanosomal TUTases.[18] *In vitro*, similarly to RET2, this latest addition to the TUTase family is exclusively U-specific and capable of both U-addition to single-stranded RNA and U-insertion into double-stranded RNA. RNAi knockdown of MEAT1 expression produced a cell-growth-inhibitory phenotype, indicating that its *in vivo* function is essential for parasite viability, as is the case for RET1 and RET2. In the mitochondrial extract, MEAT1 associates with a protein complex resembling the RNA editing core complex. In this particle, MEAT1 effectively replaces the U-insertion subcomplex, which consists of MP81 structural protein, REL2 RNA ligase, and RET2. Thus, RET2 and MEAT1 interact with similar multiprotein complexes in a mutually exclusive manner.[18] At the protein sequence level, similar to TUT4, MEAT1 does not have a middle domain, while the ~50-amino-acid insertion within the CTD can be deduced by sequence alignments with other TUTases. Finally, several active-site residues, which are invariant among trypanosomal TUTases, are replaced in MEAT1 with either similar residues (position 181; S-to-N) or those resulting in altered charge (position 140; R-to-E) or polarity (position 183; Y-to-F).

In this work, we report crystallographic and mutational analyses of MEAT1 from *T. brucei* (GenBank accession number ACT83521). X-ray structures of the apo form and UTP-bound form reveal a mechanism of UTP selection and domain organization that differs substantially from the mechanisms for previously investigated *Tb*RET2[14] and *Tb*TUT4.[6] In addition to establishing UTP-binding determinants, most of which are invariant among TUTases, we have identified and verified additional critical contributions of MEAT1-specific residues using mutagenesis. A MEAT1-specific domain, termed the bridging domain (BD), extends from the CTD and makes hydrophobic contacts with the NTD, thus creating a cavity adjacent to the UTP-binding site. Considering the similar enzymatic properties of RET2 and MEAT1 TUTases, we found that their unique domains are likely to be responsible for interactions with different protein partners and, therefore, for association with distinct functional complexes.[18]

Results

Limited proteolysis and crystallization of apo MEAT1 and UTP-bound MEAT1

Initially, crystals were obtained for full-length C-terminally and N-terminally 6His-tagged *Tb*MEAT1; however, despite numerous optimization trials, the crystal quality and diffraction resolution were poor (7 Å and 3.2 Å, respectively). In an effort to obtain higher-quality crystals, we employed limited proteolysis. Digestion with thermolysin shortened MEAT1 by approximately 4 kDa, as monitored by SDS-PAGE, leading to accumulation of a single fragment that was resistant to further degradation (Fig. 1a). Proteolyzed *Tb*MEAT1 was used without further purification to grow crystals in the presence or in the absence of UTP for data collection and structure solution. Diffraction data revealed electron density for 385 (44.3 kDa) of 406 (46.8 kDa, excluding the affinity tag) amino acids beginning with the N-terminal methionine. The remaining amino acids, along with the C-terminal His-tag, were removed by limited proteolysis with thermolysin.

All crystals belonged to space group $P2_1$ and, although the recombinant MEAT1 is a monomer in solution,[18] contained two molecules in the asymmetric unit related by 2-fold noncrystallographic symmetry. The first crystal structure was obtained from selenomethionine-labeled protein in the presence of UTP and Mg^{2+} (*Tb*MEAT1SeMet-UTP-Mg), followed by multiple anomalous dispersion phasing. Apo and UTP-bound structures were then obtained by molecular replacement using *Tb*MEAT1SeMet-UTP-Mg as search model. The resolutions achieved for *Tb*MEAT1-apo, *Tb*MEAT1-UTP, and *Tb*MEAT1-SeMet-UTP-Mg were 1.56 Å, 1.95 Å, and 2.30 Å, respectively. The stereochemistry of each model was validated by PROCHECK,[19] and the quality of these structures and data is summarized in Table 1.

Structure of *Tb*MEAT1

Notwithstanding its low sequence identity with *Tb*RET2[14] (12%) and *Tb*TUT4[6] (14%), *Tb*MEAT1 adopts a similar bidomain architecture that forms a deep cleft bearing both catalytic and nucleoside triphosphate-binding sites (Fig. 2). Global differences in the tertiary structure of UTP-bound *Tb*MEAT1 account for C^{α} r.m.s.d. values of 2.2 Å and 2.3 Å with *Tb*RET2 and *Tb*TUT4, respectively, which are significantly greater than the 1.6 Å r.m.s.d. observed between *Tb*RET2 and *Tb*TUT4.[6]

The NTD represents the DNA-polymerase-β-like (Pol β) catalytic fold containing a five-stranded anti-

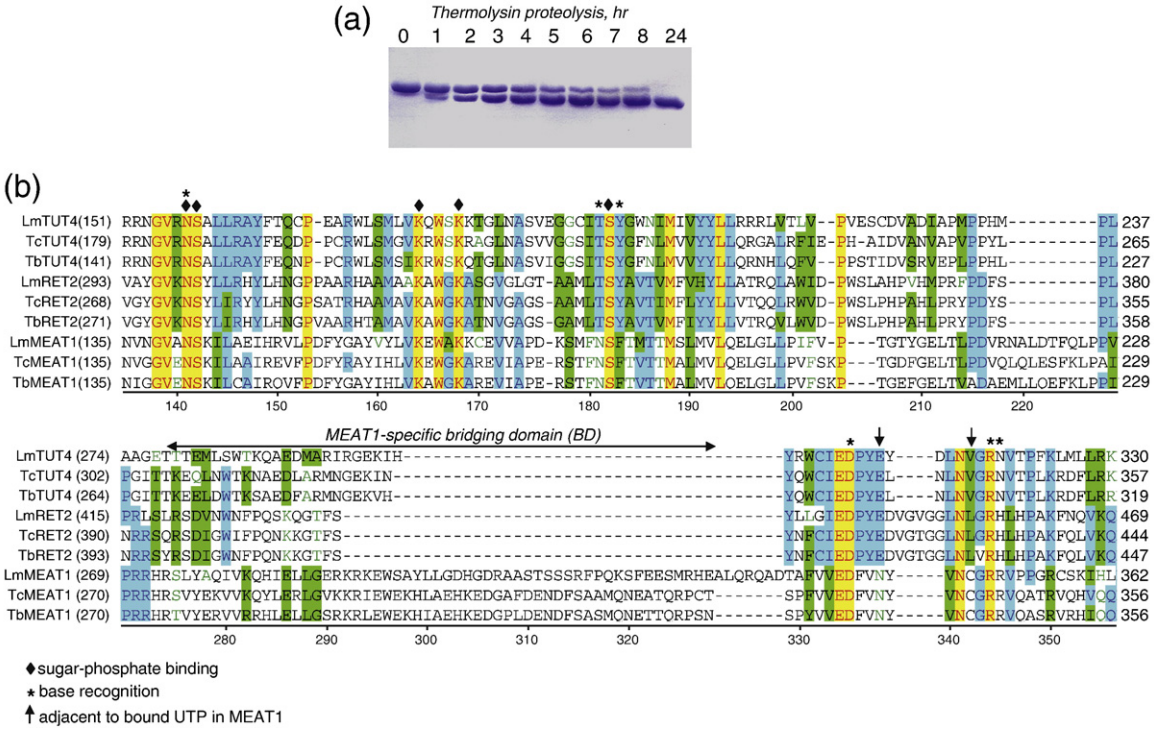

Fig. 1. Limited proteolysis of purified recombinant MEAT1. (a) Purified MEAT1 (0.5 mg/ml) was incubated at 4 °C with thermolysin (2 μg/ml) in a buffer containing 50 mM Tris–HCl (pH 8.0), 100 mM KCl, and 50 mM $CaCl_2$. Aliquots were removed at indicated periods of time, separated by SDS-PAGE, and stained with Coomassie blue. (b) Partial multiple sequence alignment of CTDs from *T. brucei* TUTases with known X-ray crystal structures (RET2,[14] TUT4,[6] and MEAT1; this study) with orthologous proteins from other Kinetoplastida species. *Lm*, *Leishmania major*; *Tc*, *Trypanosoma cruzi*; *Tb*, *T. brucei*. *Tb*MEAT1 amino acids are numbered, UTP-binding residues are depicted by diamonds (sugar–phosphate) and asterisks (uracil base), and arrows indicate MEAT1 positions adjacent to bound UTP.

Table 1. Crystal data collection and refinement statistics

Crystal data (UTP-Mg)	Remote	Peak	Inflection
Wavelength (Å)	0.97876	0.91837	0.97935
Beamline[a]	11-1	11-1	11-1
Space group	$P2_1$	$P2_1$	$P2_1$
Cell dimensions			
a (Å)	63.7	63.7	63.7
b (Å)	103.4	103.4	103.4
c (Å)	63.7	63.8	63.8
β (°)	109.6	109.6	109.6
Resolution range (Å)	50–2.30	50–2.30	50–2.30
Total reflections	254,819	251,137	251,735
Unique reflections[b]	67,571	67,371	67,988
Redundancy	3.8 (3.5)	3.7 (3.4)	3.7 (3.2)
Completeness (%)	99.6 (98.7)	99.1 (97.0)	98.9 (96.3)
Mean I/σ_I	21.7 (3.0)	21.2 (2.9)	20.3 (2.5)
R_{sym} (%)	9.2 (48.0)	9.3 (47.9)	9.3 (51.7)

Crystal data	UTP	Apo
Wavelength (Å)	0.97945	0.97945
Beamline[a]	11-1	11-1
Space group	$P2_1$	$P2_1$
Cell dimensions		
a (Å)	62.9	63.2
b (Å)	102.0	102.0
c (Å)	66.1	66.1
β (°)	111.6	112.0
Resolution range (Å)	99–1.95	99–1.56
Total reflections	193,869	394,941
Unique reflections	54,477	108,380
Redundancy	3.6 (3.0)	3.6 (3.0)
Completeness (%)	96.6 (84.0)	98.2 (90.3)
Mean I/σ_I	12.8 (2.2)	25.2 (2.0)
R_{sym} (%)	12.7 (49.1)	6.8 (53.1)

Refinement	UTP-Mg	UTP	Apo
Resolution range (Å)	31.71–2.30	31.05–1.95	31.41–1.56
Structure factors used	30,731	51,550	102,739
R_{work}/R_{free}[c] (%)	19.8/24.8	20.4/24.6	16.2/20.3
r.m.s.d. bonds (Å)	0.014	0.013	0.013
r.m.s.d. angles (°)	1.5	1.4	1.4
Number of atoms/average *B*-value (Å^2)			
Protein	6182/29.1	6261/17.4	6237/15.8[d]
Waters	170/29.2	567/26.1	879/28.8[d]
UTP	58/37.4	58/33.9	
Mg	2/32.3		
Ramachandran plot			
Favored (%)[e]	86.8	91.2	91.1
Allowed (%)[e]	13.2	8.8	8.9
Generously allowed (%)[e]	0	0	0

Values inside parentheses are calculated for the highest-resolution shell.
[a] Stanford Linear Accelerator Center (Menlo Park, CA).
[b] Bijvoet pairs separate.
[c] R_{free} based on a test set size of ca 5% of all structure factors.
[d] $B_{eq}=(8\pi^2\sum_i U_{ii})/3$ (for $i=1, 2, 3$).
[e] PROCHECK.[19]

parallel β-sheet flanked by α-helices on either side. The twisted β-sheet provides carboxylate residues (D65 and D67) that are responsible for divalent metal coordination, a feature common to all members of the Pol β superfamily. The CTD, which resembles the ATP cone domain[22] and is otherwise conserved among TUTases, contains a MEAT1-specific insertion[18] comprising two α-helices (positions 274–329). These helices fold into a compact ~6.7-kDa BD in a position that is occupied by unstructured loop regions in both *Tb*RET2 and *Tb*TUT4 (Fig. 2a). This loop region in *Tb*RET2 and *Tb*TUT4 overhangs the UTP-binding cleft and has little interaction with the remaining structure. In MEAT1, the BD interacts with the NTD, burying approximately 650 Å^2 at the interface.[23] A surface representation reveals a cavity that extends the UTP-binding cleft as a tunnel protruding from the backside of the molecule (Fig. 2b). The interface created by the BD consequently results in structural deviations in the opposing segment of the NTD relative to those regions in *Tb*RET2 (Fig. 2c) and *Tb*TUT4 (Fig. 2d).

Because MEAT1 interacts with an editosome-like complex via a binding partner that is distinct from MP81,[18] a known structural protein responsible for RET2 docking into the core editing complex,[13,24] the BD may constitute a possible interface for MEAT1 interactions *in vivo*. The superimposition of apo and UTP-bound forms of *Tb*TUT4 revealed significant conformational differences with an r.m.s.d. of 1.5 Å.[6] On the contrary, apo and UTP-bound structures of *Tb*MEAT1 are virtually identical (0.3 Å r.m.s.d.), suggesting a lack of structural rearrangement upon UTP binding. A higher relative rigidity of MEAT1 is likely caused by the additional BD-mediated interactions between the NTD and the CTD.

Structural basis for UTP binding specificity

The mode of a nucleoside's sugar–phosphate binding appears conserved among TUTases with known crystal structures. A single Mg^{2+} (or water molecule in the absence of a metal ion) is tightly coordinated by one side of the triphosphate moiety, as well as by aspartate residues 65 and 67. In the case of *Tb*MEAT1, the other side of the triphosphate is stabilized by side chains of amino acids S54, K164, K168, and S182; backbone NH groups of S54 and F183; and several ordered water molecules (Fig. 3a). The ribose 2′-hydroxyl group forms hydrogen bonds with the side-chain carbonyl oxygen of N141 and the hydroxyl group of S142 (Fig. 3b).

However, MEAT1's exclusive uracil base specificity[18] is achieved by contributions both from amino acids that are conserved among TUTases and from MEAT1-specific residues. The side-chain amide nitrogen of N141 donates a hydrogen bond to the O2 carbonyl oxygen of the uracil base (Fig. 4a). However, this hydrogen bond is slightly longer than those observed in *Tb*TUT4 and *Tb*RET2, likely because of an additional hydrogen bond with D335. In *Tb*RET2 (D421) and *Tb*TUT4 (D297), this key aspartate accepts a hydrogen bond from the hydroxyl of a conserved tyrosine (Y319 in *Tb*RET2; Y189 in *Tb*TUT4) whose aromatic ring exhibits π-stacking interactions with the uracil base (Fig. 4b). In *Tb*MEAT1, the base-stacking interaction is provided by a phenylalanine at position 183 (interplanar distance of ca 3.9 Å), and the absence of the phenol hydroxyl allows interaction between N141 and D335 (Fig. 4a). In regard to other base-specific interactions, the water molecule that interacts with N3 of the uracil does not have the restricted directionality

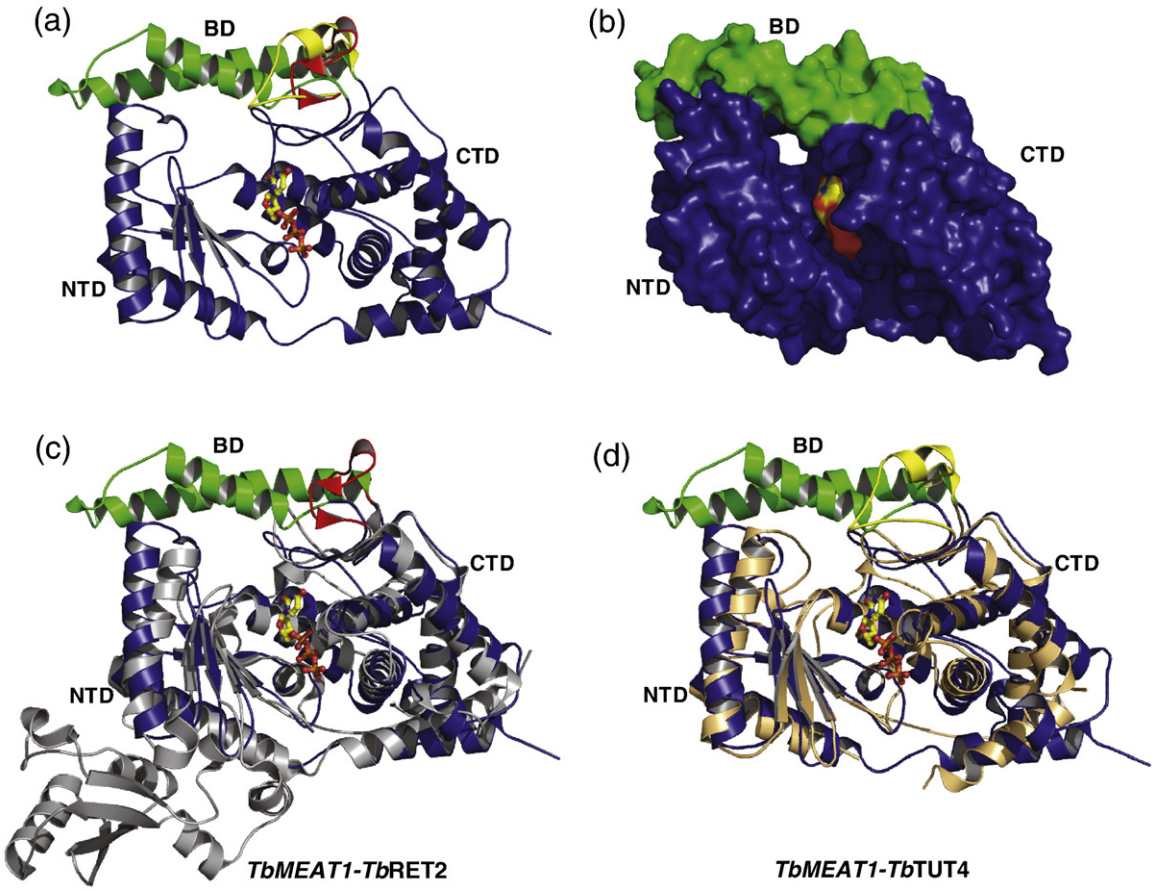

Fig. 2. Overall structure of *Tb*MEAT1. (a) Ribbon representation illustrating the UTP bound in the deep cleft formed by the NTD and the CTD. The unique two-α-helical BD (green) and its differences from the shorter regions observed in *Tb*RET2 (red) and *Tb*TUT4 (yellow) are highlighted. (b) MEAT1-UTP surface representation. Structural superpositions of *Tb*MEAT1 with (c) *Tb*RET2 (gray) and (d) *Tb*TUT4 (tan) depict the overall differences in these structures, which become increasingly evident away from the active site. Superpositions were generated with backbone α-carbons using the SSM algorithm[20] in the program Coot.[21]

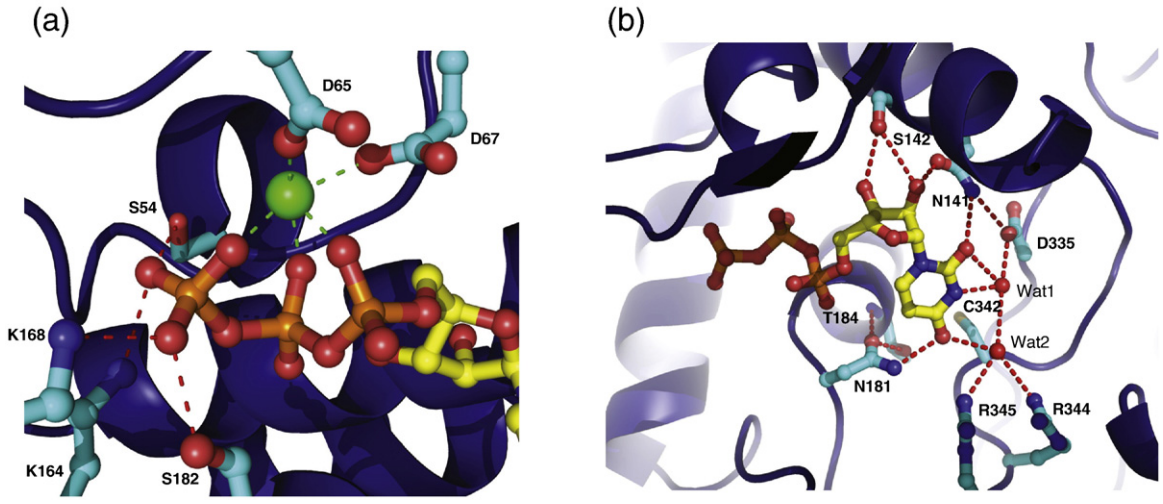

Fig. 3. *Tb*MEAT1 active site. (a) Coordination of catalytic Mg^{2+} (green) by the triphosphate of UTP and conserved aspartic acid residues. (b) The ribose sugar and uracil base moieties and their network of hydrogen bonds with neighboring active-site residues. Note MEAT1-specific N181, which donates a hydrogen bond to O4 of the uracil base. Two coordinated water molecules (Wat1 and Wat2) are included as red isolated spheres.

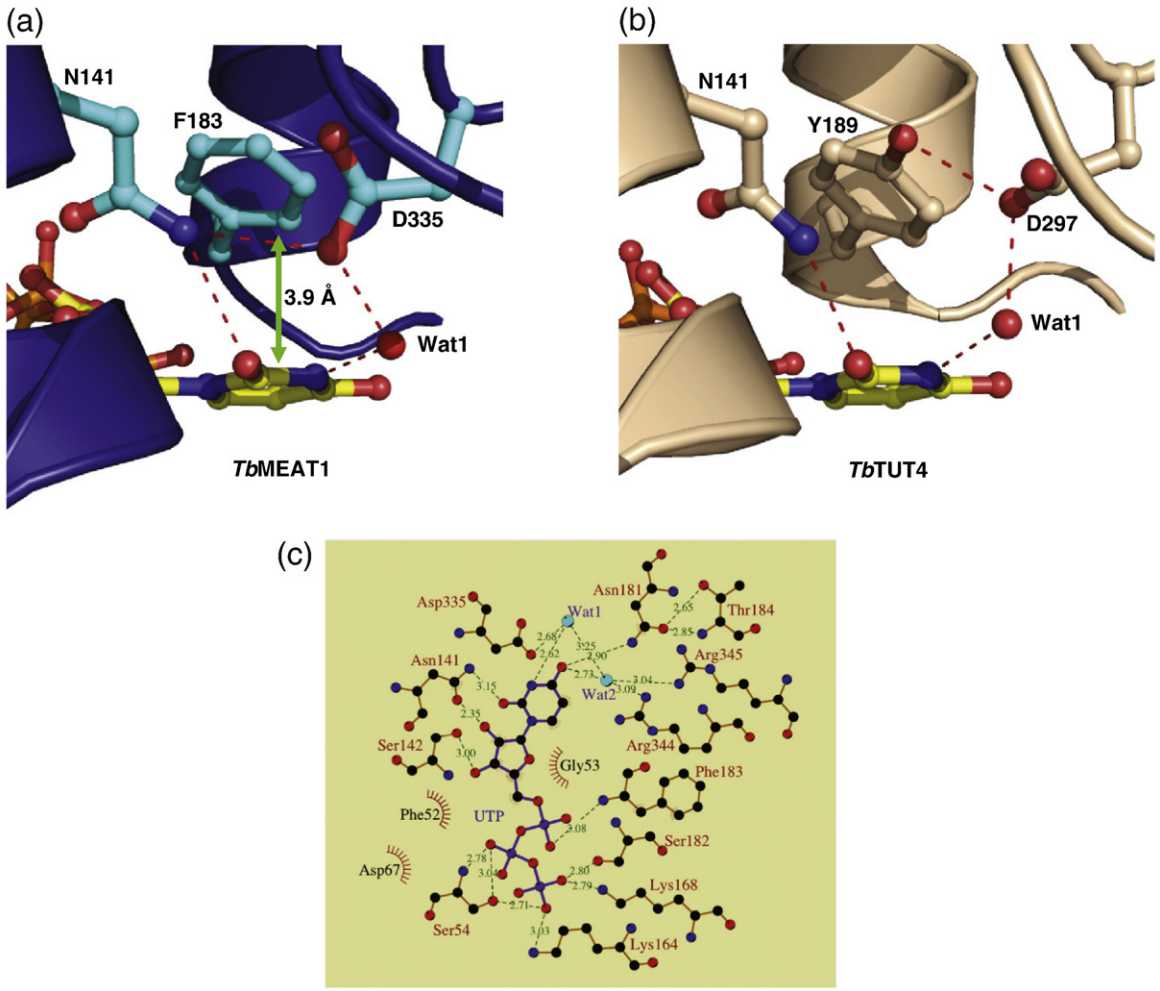

Fig. 4. Differences observed for (a) *Tb*MEAT1 and (b) *Tb*TUT4 in the conserved phenyl-containing residues involved in base-stacking interactions with bound UTP. In *Tb*TUT4, the tyrosine side chain is locked down because of hydroxyl group H-bonding with invariant D297. In *Tb*MEAT1, the corresponding position is occupied by phenylalanine 183, which enables the formation of a hydrogen bond between N141 and D335. (c) Interactions of UTP, amino acid residues, and water molecules in the MEAT1 active site. Two-dimensional representation was generated using LIGPLOT.[25]

described for the respective water molecule in *Tb*RET2 (Wat1; Fig. 5), which has been designated as *Tb*RET2's primary basis for U-specificity.[14] Furthermore, glutamate 424 of *Tb*RET2, which together with D421 facilitates the hydrogen-bonding pattern observed for Wat1, is replaced by an asparagine (N338) in *Tb*MEAT1. This side chain has no apparent involvement in nucleoside binding, but may play a structural role. On the other hand, the invariant arginine in position 344, together with MEAT1-specific R345, coordinates a water molecule (Wat2) (*B*-factor = 27.1 Å^2), which donates a hydrogen bond to O4 of the uracil base and also H-bonds with Wat1 (*B*-factor = 26.4 Å^2) (Figs. 3b and 5).

Perhaps the most significant feature that confers U-specificity to *Tb*MEAT1 by means alternative to *Tb*RET2 and *Tb*TUT4 is the contribution of N181 at a position universally occupied by serine in other trypanosomal TUTases. The side-chain amide nitrogen of N181 donates a hydrogen bond directly to O4 of the uracil base (Figs. 3b and 5). The side-chain carbonyl oxygen of N181 is locked by H-bonds from the backbone NH and side-chain hydroxyl of T184, thus making it energetically unfavorable for the side chain to adopt the opposite rotamer as would be preferred in the case of the cytosine nucleotide base. The threonine in position 184 apparently covaries with N181 in MEAT1 sequences from different trypanosomal species; in other TUTases, the position corresponding to T184 is occupied by alanines or glycines, which possess small nonpolar side chains incapable of H-bonding (Fig. 1b).

Binding of alternative substrates

MEAT1[18] and TUT4[6] TUTases show preferences for single-stranded RNA substrates with Us at their 3′-end, while RET2[15] is more active in RNAs with terminal purines. Conversely, MEAT1 and RET2 are exclusively U-specific, while TUT4 also incorporates CTP (although with lower efficiency) and residual levels of ATP and GTP. Cocrystallization and crystal

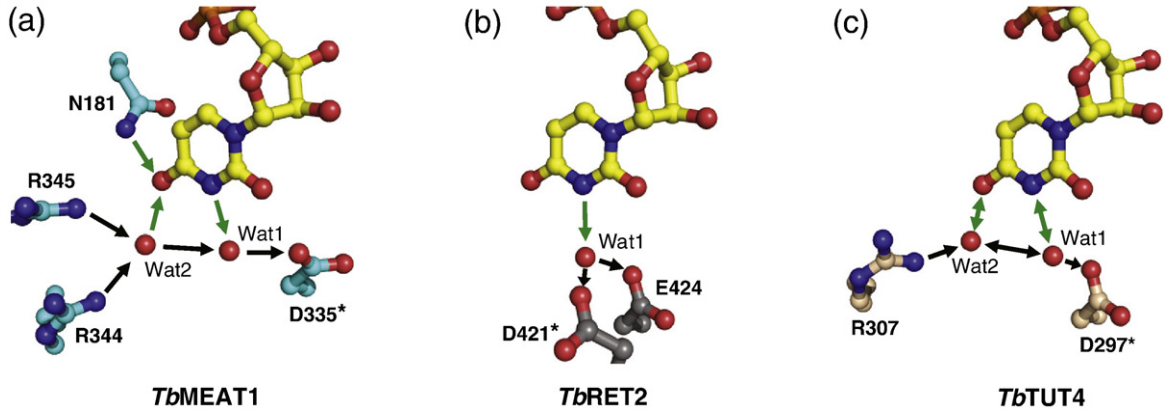

Fig. 5. Comparison of the structural bases for achieving UTP specificity by *Tb*MEAT1 (a), *Tb*RET2 (b), and *Tb*TUT4 (c) TUTases. Models were generated from Protein Data Bank codes 3HJ1, 2B51, and 2IKF, respectively. Hydrogen bonds involved in uracil-base-specific interactions are depicted as green arrows. Invariant aspartic acid residues are indicated by asterisks.

soaking experiments with various NTPs and mononucleotides/dinucleotides serving as minimal RNA substrates demonstrated that, at physiological NTP concentrations, *Tb*TUT4 binds all four nucleoside triphosphates. However, the coplanarity of purine bases relative to pyrimidines was suboptimal for both stacking interactions with the invariant aromatic residue (Y189) and the terminal base of the RNA substrate. These observations led to a model suggesting that the specificity of U-addition by TUT4 is achieved via uracil base binding in a specific orientation, which in turn creates a binding interface for the terminal RNA base.[15] However, soaking RET2 crystals in non-UTP substrates revealed only a partial occupancy in the sugar–phosphate region, but virtually no density corresponding to nucleotide bases. RET2's specificity, therefore, was explained based entirely on protein–UTP interactions.[14]

To distinguish which of these mechanisms is applicable to *Tb*MEAT1, we solved structures of *Tb*MEAT1 crystallized in the presence of ATP, GTP, and CTP. Similar to *Tb*RET2, only partial occupancy was observed for each of these nucleoside triphosphates, with electron density peaking at the triphosphate moiety and diminishing toward the nucleotide bases (data not shown). Furthermore, unlike with *Tb*TUT4, soaking of *Tb*MEAT1-UTP crystals with high concentrations of UMP or UpU, as well as cocrystallization attempts of *Tb*MEAT1 with UpU, revealed no electron density for UMP or UpU in either case. Nonetheless, the universal metal ion coordination by D65 and D67 suggests that RNA binding creates a pocket for the second metal, which in turn activates 3′-OH as nucleophile. In conclusion, it is likely that although the mechanisms of UTP recognition by *Tb*MEAT1 and *Tb*RET2 are only partially conserved, in both cases, uracil base specificity is achieved by direct or water-mediated contacts of the uracil base in the respective binding sites.

Mutational analysis of the UTP-binding site

Because of considerable differences in the architecture of the uracil-binding sites among *Tb*MEAT1 and previously studied TUTases, we next determined the effects of point mutations introduced at positions that are invariant among TUTases, as well as those occupied by MEAT1-specific residues. To ensure that the effects of these mutations were examined within the context of the same molecule used in crystallographic analysis, we genetically engineered a C-terminally truncated protein to match a removal of 25 amino acids by thermolysin digestion (Fig. 6a). As demonstrated by comparison of U-addition profiles, neither limited proteolysis nor genetically engineered C-terminal deletion had any discernable effects on enzymatic activity. A moderate lengthening of extension products for the truncated MEAT1 at a longer incubation time was likely caused by increased protein stability (Fig. 6b).

A triad of carboxyl residues (D65, D67, and D130; MEAT1 numbering), two of which are part of the signature sequence hG[G/S]x(9,13)Dh[D/E]h (where x is any amino acid and h is a hydrophobic residue) and the third positioned in close spatial proximity, represents a conserved functional assembly in TUTases and most other members of the Pol β superfamily. Predictably, substitution of D67, which is part of the catalytic metal-binding shell, led to complete elimination of MEAT1 activity (Fig. 6c). Position N141 is universally conserved among TUTases, as the asparagine's side-chain carbonyl group is involved in the recognition of the ribose ring, while its side-chain amide group donates a hydrogen bond to O2 of the uracil base. The corresponding alanine substitution decreased the catalytic efficiency of *Tb*TUT4 by ~100-fold,[6] while the N141A mutation caused an approximately 10-fold drop in the k_{cat}/K_m value for MEAT1 (Fig. 6c; data not shown). The effects of mutating another invariant residue (R307 in TUT4[6] and R344 in MEAT1) that is engaged in water-mediated contact with O4 of the uracil moiety were also very consistent among these two divergent TUTases: a decline in catalytic efficiency by ~20-fold (Fig. 6c). Finally, the key determinants of uracil base binding[6] (an aromatic ring at position 183 and aspartic acid in position 335), which provide π-stacking interactions

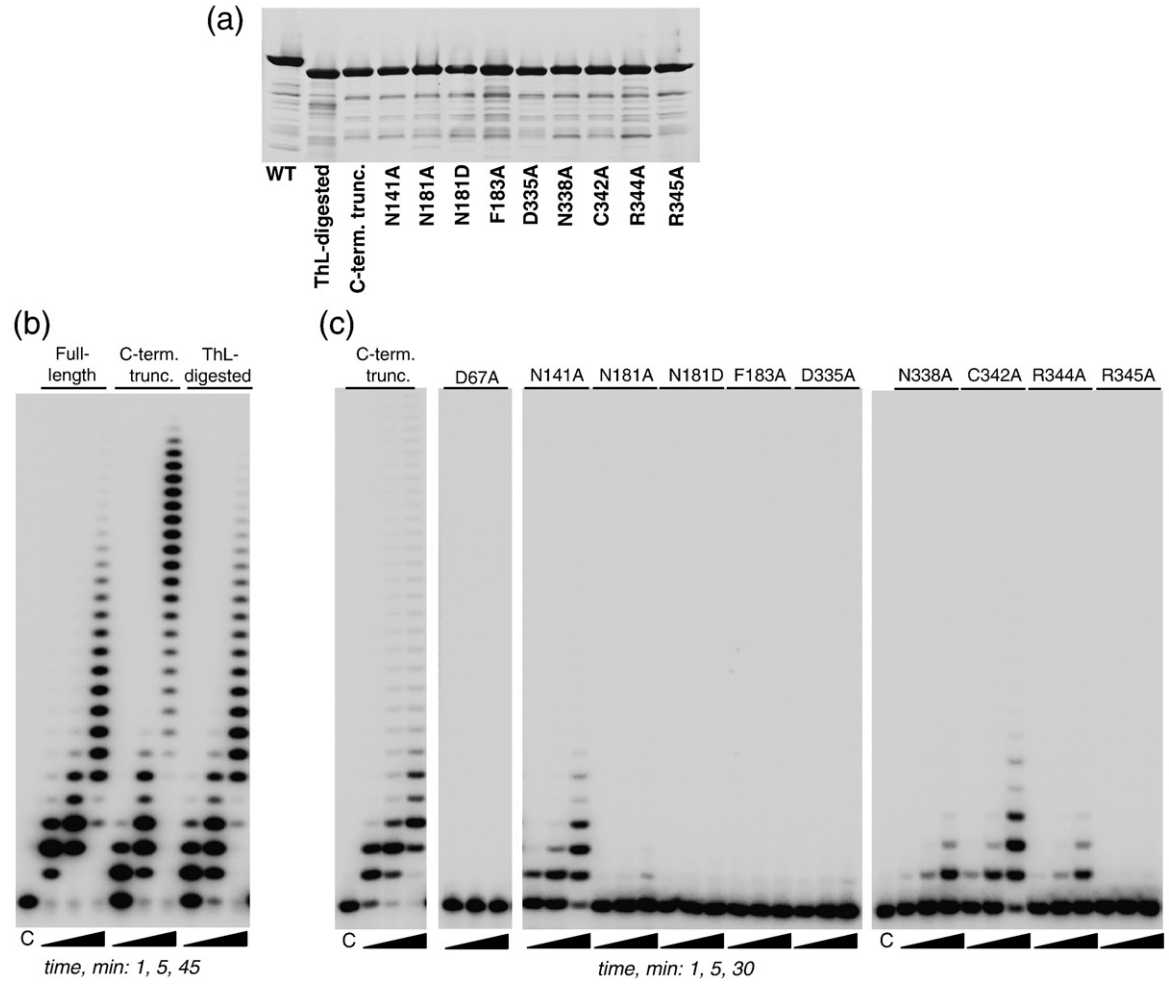

Fig. 6. Effects of catalytic site mutations on U-addition activity. (a) Purified mutant proteins were separated on SDS gels and stained with Sypro Ruby. (b) U-addition patterns for full-length *Tb*MEAT1, a genetically engineered C-terminal truncated form, and the thermolysin-resistant fragment. Reactions were performed in the presence of 300 nM MEAT1, 100 μM UTP, and 1 μM RNA for indicated periods of time under the conditions described in Materials and Methods. Products were separated on a 15% acrylamide/8 M urea gel. (c) U-addition activity of mutant proteins. Assays were carried out as in (b).

and coordination of the water molecule (Wat1) receiving an H-bond from position 3, respectively, appear to be essential for MEAT1 activity: corresponding alanine substitutions inactivated the enzyme (Fig. 6c).

Next we analyzed amino acids that are divergent between MEAT1 and other TUTases (Fig. 1b) and are located within immediate proximity of the bound UTP (C342 and N338), as well as those that contact UTP directly or via coordinated water molecules (N181 and R345). The thiol group of C342 is positioned within 4 Å (or closer for some rotamers) of O4 of the uracil and, unlike hydrophobic amino acids in other TUTases, has a potential to form an H-bond with the base (Fig. 3b). The contribution of this interaction, however, appears to be insignificant as the C342A mutation had only a minor inhibitory effect. Unlike glutamate 424 in RET2, which is essential for coordination of Wat1 and uracil recognition (Fig. 5), in MEAT1, the corresponding asparagine residue in position 338 is tightly fixed by intraprotein hydrogen bonds and provides no apparent contribution to UTP binding. Therefore, the moderate inhibitory effect of alanine substitution manifested by a ~20-fold lower catalytic efficiency (Fig. 6c) was likely caused by structural permutations.

The asparagine in position 181 (occupied by serine in other TUTases) and the arginine in position 345 (typically glutamine or histidine in other TUTases) clearly contribute the most critical uracil base contacts among the MEAT1-specific amino acids tested in this study. The N181A mutation virtually eliminated TUTase activity, and its effect could not be rescued by N181D substitution, indicating that the amide contribution made by H-bonding to O4 is essential for UTP binding (Figs. 3b, 5a, and 6c). In TUT4 and RET2, O4 receives a single H-bond, and disruption of this interaction by R307A mutation led only to moderate inhibition of TUT4 activity.[6] Thus, the deleterious effect of the R345A mutation, which presumably eliminates Wat2-mediated H-bonding

(Figs. 3b, 5a, and 6c), further establishes O4 as the key element recognized by MEAT1. A direct interaction between R345 and O4 of the uracil base would be limited to a dipole–dipole interaction as the distance is too long for hydrogen bonding (3.6 Å).

Finally, testing of all mutant proteins for CTP, ATP, and GTP incorporation activity provided no indications that removal of UTP-specific positive-binding determinants relaxes MEAT1 specificity (data not shown). In conclusion, the atomic mechanism that ensures exclusive UTP binding by MEAT1 is a combination of hydrogen bonds and π-stacking interactions, which are likely universal among the TUTase enzyme family, as well as additional H-bonds provided by MEAT1-specific residues.

Discussion

The structural and functional diversity of RNA uridylyl transferases in trypanosomes provided early recognition of 3′-uridylylation as a widespread posttranscriptional RNA modification with a profound impact on eukaryotic RNA processing.[1,26] Recent reports demonstrate that TUTases participate in processes as diverse as U6 snRNA 3′-end processing,[27] cell-cycle-dependent regulation of histone mRNA stability in human cells,[28] accelerated decay of let-7 micro RNA precursor,[29] 3′-uridylylation of actin mRNAs in *Schizosaccharomyces pombe*,[30] and degradation of mRNA cleavage fragments in plants.[31] Because three trypanosomal TUTases (RET1, RET2, and MEAT1) are essential for parasite viability and because human Zcchc11 TUTase has implications in cancer and stem cell biology,[32] the structures of TUTase active sites and mechanisms of UTP selection are of substantial interest from a pharmaceutical standpoint.

Crystallographic studies of trypanosomal RET2[14] and TUT4[6,15] TUTases underscored a conserved bidomain organization of the catalytic core and conservation of the key UTP-binding residues. However, significant differences were observed in the mechanisms of UTP selection. Whereas RET2, an exclusively U-specific enzyme active on double-stranded RNA, apparently relies entirely on protein–UTP contacts, the less specific TUT4 invokes active participation of the single-stranded RNA substrate to select a cognate nucleoside triphosphate.

Here we report crystallographic and mutational analyses of a recently identified third trypanosomal mitochondrial TUTase, MEAT1. Crystal structures were solved for the apo, UTP-Mg^{2+}-bound, and UTP-Mg^{2+}-bound forms at moderate to high resolution. In contrast to TUT4, these structures are virtually identical, indicating a lack of appreciable conformational changes upon UTP binding. The overall fold of the globular bidomain formed by the NTD and the CTD in MEAT1 is similar to those of *Tb*RET2 and *Tb*TUT4. In MEAT1, however, the CTD contains an insertion of two α-helices that form a bridge extending across the top of the UTP-binding cleft and interacting with the NTD. This additional BD likely confers greater stability to the entire fold, but may also be involved in protein–protein interactions responsible for docking of MEAT1 into the editosome-like complex. The MEAT1-associated particle closely resembles the RNA editing core complex (also referred to as the 20S editosome), but lacks RET2 TUTase. Although specific RNA substrates of MEAT1 and the MEAT1-associated complex remain to be firmly established, RNA interference studies demonstrated that MEAT1 expression is essential for the viability of parasites both in the bloodstream and in procyclic forms.

The *in vitro* experiments demonstrate that TUTases differ substantially in their NTP selectivity: from U-specific (RET2 and MEAT1) to moderate incorporation of CTP (RET1 and TUT4), to being equally active in both U-addition and A-addition (Cid1 from *S. pombe*).[33] Accordingly, TUTases and ncPAPs[34] are not readily distinguishable at the protein sequence level. Furthermore, existing evidence suggests that the nucleotide specificity of TUTases may be affected by interacting partners and/or the structures of RNA substrates *in vivo*.[35,36] The trypanosomal mitochondrial poly(A) polymerase KPAP1, for example, is highly similar to TUTases; most positions involved in UTP binding are also conserved in KPAP1.[3] It is therefore not surprising that the active sites of TUTases, and perhaps of noncanonical poly(A) polymerases, are quite spacious and that steric constraints do not appear to be discriminating factors between purine and pyrimidine bases. Instead, positive determinants (direct or water-mediated hydrogen-bonding and π-stacking interactions) are exploited to select UTP even though the atomic details of uracil recognition vary among TUTases. *Tb*RET2 employs unidirectional hydrogen bonding via a water molecule;[14] *Tb*TUT4 prefers UTP over CTP, with no obvious reason for selection of the former;[6,15] and *Tb*MEAT1 relies on unidirectional hydrogen bonding via an active-site asparagine (Fig. 5). Whereas the promiscuity in nucleoside binding observed for *Tb*TUT4 may explain its lower selectivity in U-addition reactions, the differences between *Tb*RET2 and *Tb*MEAT1 are rather intriguing, as both are exclusively U-specific, are localized to the mitochondrion, and associate with similar yet distinct complexes.

The mechanism for nucleoside incorporation involves nucleophilic attack by 3′-OH of the terminal RNA residue on the α-phosphorus atom of the bound nucleoside triphosphate. The nucleophilic substitution reaction is catalyzed by the tightly coordinated Mg^{2+}, which stabilizes the pyrophosphate-leaving group. Adaptation of this mechanism for TUTases has been demonstrated by the crystal structure of *Tb*TUT4 with bound UTP and UMP, in which UMP models the terminal nucleoside of an RNA substrate.[15] In this example, a second Mg^{2+} catalyst, which was not observed in the *Tb*TUT4-UTP binary complex, brings the nucleophile and electrophile into reacting proximity. This

mechanism also implicates an active role for the RNA substrate in pyrimidine selectivity through subsequent base-stacking interactions between the terminal nucleoside base and the bound pyrimidine base. However, soaking of *Tb*MEAT1-UTP cocrystals with UMP revealed no electron density for UMP. This may imply that MEAT1 requires a longer RNA substrate for productive binding or that UTP–protein contacts are indeed sufficient to confer the observed UTP selectivity. In the latter scenario, coordination of the uracil's O4 via additional hydrogen bonding from MEAT1-specific N181 (an interaction not seen in RET2 or TUT4), as well as via stacking interaction and hydrogen bonding involving position N3 of the uracil base, appears to be a critical contribution.

Furthering our understanding of the mechanisms by which TUTases edit RNA and regulate gene expression will enable exploration of these vital processes for trypanocide development. Specifically, atomic details of RET2 and MEAT1 active sites can be exploited for *in silico* docking to identify potential TUTase inhibitors.

Materials and Methods

Mutagenesis, expression, and purification of recombinant MEAT1

C-terminally 6His-tagged *Tb*MEAT1 was expressed in *Escherichia coli* strain BL21(DE3) RIL Codon plus (Stratagene) using M9 minimal media. The cells were grown at 37 °C to an A_{600} of 0.7–0.8 and reduced to a temperature below 18 °C, and expression was induced with 1 mM IPTG for 2 days at 10 °C. The expression protocol for selenomethionine labeling was the same, except for the use of the B834(DE3) methionine auxotroph strain (Novagen) and supplementation of the media with 60 mg/L L-selenomethionine prior to induction and with another 60 mg/L L-selenomethionine 24 h after induction. Cell pellets were washed with phosphate-buffered saline; resuspended in 7.5 ml/g cell mass of lysis buffer containing 50 mM Hepes (pH 8.0), 50 mM NaCl, 1 mg/ml lysozyme, and one tablet of Complete EDTA-Free (Roche) protease inhibitors; and passed through a French Press at 1000 psi. The cellular extract was adjusted to 300 mM NaCl and 0.1% Triton X-100, and clarified by centrifugation at 40,000*g*. The protein was purified by loading onto a 5-ml bed volume of TALON (Clontech) affinity resin and washing with 10 column volumes of 50 mM Hepes (pH 8.0) and 300 mM NaCl, followed by 10 column volumes of a more stringent wash with the same buffer containing 10 mM imidazole. The protein was eluted from the column in 50 mM Hepes (pH 8.0), 300 mM NaCl, and 200 mM imidazole. Fractions from the TALON column were pooled; diluted 6-fold with 25 mM Tris–HCl (pH 8.0) and 1 mM DTT; and loaded onto a 5-ml HiTrap Q HP anion-exchange column (GE Healthcare). The column was washed with 10 column volumes of 25 mM Tris–HCl (pH 8.0), 1 mM DTT, and 50 mM NaCl, and eluted using the same buffer with a linear gradient of NaCl from 0.05 M to 1 M over 20 column volumes. Fractions were analyzed by SDS-PAGE and stained with Sypro Ruby.

Point mutations were introduced by a PCR-based method using the QuikChange XL kit (Stratagene) and confirmed by DNA sequencing. Mutant proteins were isolated from 2 L of bacterial culture, as described previously.

Limited proteolysis and sample preparation

Purified fractions were diluted to achieve a 100 mM concentration of NaCl, and glycerol and $CaCl_2$ were added to 5% and 50 mM, respectively. Thermolysin (Sigma) was added at a ratio of 1:250 (weight of protease/weight of substrate), and the reaction was carried out at 4 °C for 24 h. The cleaved protein was subsequently dialyzed against 2 L of 50 mM Hepes (pH 8.0), 100 mM NaCl, 5% glycerol, 1 mM DTT, and 1 mM ethylenediaminetetraacetic acid for 4 h, and again in another 2 L of dialysis buffer for 16 h. 3-[(3-Cholamidopropyl)dimethylammonio]propanesulfonic acid was added to 0.3% (wt/vol), and the protein was concentrated to 10 mg/ml using a Centricon centrifugal filter device (Amicon) with a molecular weight cutoff of 10,000.

Crystallization and structure solution

The crystals were grown at 18 °C at a protein concentration of 5 mg/ml and a 0-fold to 5-fold molar excess of UTP in a crystallization buffer containing 0.2 M lithium acetate and 25% polyethylene glycol 3350, using the hanging-drop vapor-diffusion method. Crystals were soaked for 1–5 min in a similar crystallization buffer containing 30% polyethylene glycol 3350, supplemented with 15% glycerol as cryoprotectant, and flash-cooled in liquid N_2. Initial crystals of full-length C-terminally and N-terminally His-tagged *Tb*MEAT1 diffracted to 7 Å and 3.2 Å, respectively. Data for the proteolyzed *Tb*MEAT1-UTP cocrystal were collected to 1.95 Å resolution. Numerous attempts of molecular replacement using various search models of *Tb*TUT4 and *Tb*RET2 were unsuccessful. Selenomethionine-labeled protein was then generated and crystallized under the same conditions; crystals were soaked in the same cryoprotectant solution with 10 mM $MgCl_2$ (*Tb*MEAT1SeMet-UTP-Mg). Data were collected at the Se peak, inflection, and remote wavelengths, and the structure was solved by three-wavelength multiple anomalous dispersion to 2.30 Å resolution. The program SOLVE[37] was used to locate the positions of selenium atoms and to compute the initial phases. Electron density was improved using RESOLVE,[38,39] followed by further density modification in DM.[23] The structure factors and improved phases were utilized in Buccaneer software[40] for automated building of a virtually complete model. The apo structure (*Tb*MEAT1-apo) was obtained in an unsuccessful attempt to cocrystallize the enzyme with UpU bound in the active site. Crystals of this type, which were grown in the presence of a 2-fold molar excess of UpU under the same crystallization conditions, exhibited a significant improvement in resolution (1.56 Å), yet were devoid of electron density for the substrate in the active site. All data were processed in HKL2000,[18] and model building was carried out with Coot.[21] Refmac5[41] was employed for restrained refinement with TLS parameters, and NCS restraints were applied to the entire molecule. *Tb*MEAT1-apo was refined using anisotropic *B*-factors, and hydrogens were generated for refinement but not included in the model. Due to nonisomorphism, the starting models of *Tb*MEAT1-UTP and *Tb*MEAT1-apo were generated by molecular replacement using the program PHASER[42] and using *Tb*MEAT1SeMet-UTP-Mg as search model. The test set was conserved for the

*Tb*MEAT1-UTP and *Tb*MEAT1-apo structures. All figures were generated using PyMOL†.

Cocrystallization and crystal soaking with alternative substrates

Cocrystallization attempts of *Tb*MEAT1 with ATP, GTP, and CTP, containing a 5-fold molar excess of NTPs, were carried out under the same conditions as with UTP. For attempts at UMP and UpU binding, *Tb*MEAT1-UTP cocrystals were soaked in cryoprotecting solution containing either 10 mM UMP or 1 mM UpU, with soaking times ranging from 30 min to several hours. Data were collected, processed, and utilized to generate electron density maps in a similar manner as previously mentioned.

Enzymatic assays

Reactions were performed in a buffer containing 50 mM Tris–HCl (pH 8.0), 1 mM DTT, 10 mM KCl, 10 mM MgAc, and 0.5 μM RNA of 5′-labeled RNA substrate (5′GCUAUGUCUGUCAACUUGUUUUUU-3′) at 27 °C for 1–45 min. Reactions were started by adding recombinant proteins to 50–300 nM and stopped by adding 1.5 vol of 10 mM ethylenediaminetetraacetic acid/95% formamide solution. Products were separated on a 15% acrylamide/8 M urea gel. Initial velocities for U-addition were determined at UTP concentrations ranging from 0.5 μM to 150 μM and with reaction times from 1 min to 20 min. Quantity One software was used to calculate the intensities of input and product bands. Steady-state kinetic parameters were obtained using the enzyme kinetics module in the Sigma Plot package.

Protein Data Bank accession codes

The structure factors and atomic coordinates for *Tb*MEAT1-UTP-Mg, *Tb*MEAT1-UTP, and *Tb*MEAT1-apo have been deposited with the RCSB Protein Data Bank under accession codes 3HIY, 3HJ1, and 3HJ4, respectively.

Acknowledgements

We thank Elena Galitovskaya for technical assistance and members of the Luecke and Aphasizhev laboratories for discussions. This work was supported by the UCI Center for Biomembrane Systems and National Institutes of Health grants R01 AI078000 (to H.L.) and RO1 AI064653 (to R.A.).

References

1. Aphasizhev, R. & Aphasizheva, I. (2008). Terminal RNA uridylyltransferases of trypanosomes. *Biochim. Biophys. Acta*, **1779**, 270–280.
2. Etheridge, R. D., Clemens, D. M. & Aphasizhev, R. (2009). Identification and characterization of nuclear non-canonical poly(A) polymerases from *Trypanosoma brucei*. *Mol. Biochem. Parasitol.* **164**, 66–73.
3. Etheridge, R. D., Aphasizheva, I., Gershon, P. D. & Aphasizhev, R. (2008). 3′ Adenylation determines mRNA abundance and monitors completion of RNA editing in *T. brucei* mitochondria. *EMBO J.* **27**, 1596–1608.
4. Kao, C. Y. & Read, L. K. (2007). Targeted depletion of a mitochondrial nucleotidyltransferase suggests the presence of multiple enzymes that polymerize mRNA 3′ tails in *Trypanosoma brucei* mitochondria. *Mol. Biochem. Parasitol.* **154**, 158–169.
5. Aphasizhev, R., Aphasizheva, I. & Simpson, L. (2004). Multiple terminal uridylyltransferases of trypanosomes. *FEBS Lett.* **572**, 15–18.
6. Stagno, J., Aphasizheva, I., Rosengarth, A., Luecke, H. & Aphasizhev, R. (2007). UTP-bound and apo structures of a minimal RNA uridylyltransferase. *J. Mol. Biol.* **366**, 882–899.
7. Aphasizhev, R., Sbicego, S., Peris, M., Jang, S. H., Aphasizheva, I., Simpson, A. M. *et al.* (2002). Trypanosome mitochondrial 3′ terminal uridylyl transferase (TUTase): the key enzyme in U-insertion/deletion RNA editing. *Cell*, **108**, 637–648.
8. Aphasizhev, R., Aphasizheva, I., Nelson, R. E., Gao, G., Simpson, A. M., Kang, X. *et al.* (2003). Isolation of a U-insertion/deletion editing complex from *Leishmania tarentolae* mitochondria. *EMBO J.* **22**, 913–924.
9. Panigrahi, A. K., Schnaufer, A., Ernst, N. L., Wang, B., Carmean, N., Salavati, R. & Stuart, K. (2003). Identification of novel components of *Trypanosoma brucei* editosomes. *RNA*, **9**, 484–492.
10. Aphasizheva, I. & Aphasizhev, R. (2010). RET1-catalyzed uridylylation shapes the mitochondrial transcriptome in *Trypanosoma brucei*. *Mol. Cell. Biol.* **30**, 1555–1567.
11. Simpson, L., Aphasizhev, R., Lukes, J. & Cruz-Reyes, J. (2010). Guide to the nomenclature of kinetoplastid RNA editing: a proposal. *Protist*, **161**, 2–6.
12. Aphasizhev, R., Aphasizheva, I. & Simpson, L. (2003). A tale of two TUTases. *Proc. Natl Acad. Sci. USA*, **100**, 10617–10622.
13. Ernst, N. L., Panicucci, B., Igo, R. P., Jr., Panigrahi, A. K., Salavati, R. & Stuart, K. (2003). TbMP57 is a 3′ terminal uridylyl transferase (TUTase) of the *Trypanosoma brucei* editosome. *Mol. Cell*, **11**, 1525–1536.
14. Deng, J., Ernst, N. L., Turley, S., Stuart, K. D. & Hol, W. G. (2005). Structural basis for UTP specificity of RNA editing TUTases from *Trypanosoma brucei*. *EMBO J.* **24**, 4007–4017.
15. Stagno, J., Aphasizheva, I., Aphasizhev, R. & Luecke, H. (2007). Dual role of the RNA substrate in selectivity and catalysis by terminal uridylyl transferases. *Proc. Natl Acad. Sci. USA*, **104**, 14634–14639.
16. Aphasizheva, I., Aphasizhev, R. & Simpson, L. (2004). RNA-editing terminal uridylyl transferase 1: identification of functional domains by mutational analysis. *J. Biol. Chem.* **279**, 24123–24130.
17. Ringpis, G. E., Aphasizheva, I., Wang, X., Huang, L., Hatfield, G. W. & Aphasizhev, R. (2010). Mechanism of RNA editing in trypanosome mitochondria: the bimodal U-insertion activity of the core complex. *J. Mol. Biol.* 2010 Apr 1. [Epub ahead of print].
18. Aphasizheva, I., Ringpis, G. E., Weng, J., Gershon, P. D., Lathrop, R. H. & Aphasizhev, R. (2009). Novel TUTase associates with an editosome-like complex in mitochondria of *Trypanosoma brucei*. *RNA*, **15**, 1322–1337.
19. Laskowski, R. A., Macarthur, M. W., Moss, D. S. & Thornton, J. M. (1993). PROCHECK—a program to

† http://www.pymol.org

check the stereochemical quality of protein structures. *J. Appl. Crystallogr.* **26**, 283–291.
20. Krissinel, E. & Henrick, K. (2004). Secondary-structure matching (SSM), a new tool for fast protein structure alignment in three dimensions. *Acta Crystallogr. Sect. D*, **60**, 2256–2268.
21. Emsley, P. & Cowtan, K. (2004). Coot: model-building tools for molecular graphics. *Acta Crystallogr. Sect. D*, **60**, 2126–2132.
22. Aravind, L., Wolf, Y. I. & Koonin, E. V. (2000). The ATP-cone: an evolutionarily mobile, ATP-binding regulatory domain. *J. Mol. Microbiol. Biotechnol.* **2**, 191–194.
23. Bailey, S. (1994). The CCP4 suite—programs for protein crystallography. *Acta Crystallogr. Sect. D*, **50**, 760–763.
24. Schnaufer, A., Ernst, N. L., Palazzo, S. S., O'Rear, J., Salavati, R. & Stuart, K. (2003). Separate insertion and deletion subcomplexes of the *Trypanosoma brucei* RNA editing complex. *Mol. Cell*, **12**, 307–319.
25. Wallace, A. C., Laskowski, R. A. & Thornton, J. M. (1995). LIGPLOT: a program to generate schematic diagrams of protein–ligand interactions 4. *Protein Eng.* **8**, 127–134.
26. Aphasizhev, R. (2005). RNA uridylyltransferases. *Cell Mol. Life Sci.* **62**, 2194–2203.
27. Trippe, R., Guschina, E., Hossbach, M., Urlaub, H., Luhrmann, R. & Benecke, B. J. (2006). Identification, cloning, and functional analysis of the human U6 snRNA-specific terminal uridylyl transferase. *RNA*, **12**, 1494–1504.
28. Mullen, T. E. & Marzluff, W. F. (2008). Degradation of histone mRNA requires oligouridylation followed by decapping and simultaneous degradation of the mRNA both 5′ to 3′ and 3′ to 5′. *Genes Dev.* **22**, 50–65.
29. Heo, I., Joo, C., Kim, Y. K., Ha, M., Yoon, M. J., Cho, J. *et al.* (2009). TUT4 in concert with Lin28 suppresses microRNA biogenesis through pre-microRNA uridylation. *Cell*, **138**, 696–708.
30. Rissland, O. S. & Norbury, C. J. (2009). Decapping is preceded by 3′ uridylation in a novel pathway of bulk mRNA turnover. *Nat. Struct. Mol. Biol.* **16**, 616–623.
31. Shen, B. & Goodman, H. M. (2004). Uridine addition after microRNA-directed cleavage. *Science*, **306**, 997.
32. Hagan, J. P., Piskounova, E. & Gregory, R. I. (2009). Lin28 recruits the TUTase Zcchc11 to inhibit let-7 maturation in mouse embryonic stem cells. *Nat. Struct. Mol. Biol.* **16**, 1021–1025.
33. Read, R. L., Martinho, R. G., Wang, S. W., Carr, A. M. & Norbury, C. J. (2002). Cytoplasmic poly(A) polymerases mediate cellular responses to S phase arrest. *Proc. Natl Acad. Sci. USA*, **99**, 12079–12084.
34. Houseley, J., LaCava, J. & Tollervey, D. (2006). RNA-quality control by the exosome. *Nat. Rev. Mol. Cell Biol.* **7**, 529–539.
35. Mellman, D. L., Gonzales, M. L., Song, C., Barlow, C. A., Wang, P., Kendziorski, C. & Anderson, R. A. (2008). A PtdIns4,5P2-regulated nuclear poly(A) polymerase controls expression of select mRNAs. *Nature*, **451**, 1013–1017.
36. Rissland, O. S., Mikulasova, A. & Norbury, C. J. (2007). Efficient RNA polyuridylation by noncanonical poly(A) polymerases. *Mol. Cell Biol.* **27**, 3612–3624.
37. Terwilliger, T. C. & Berendzen, J. (1999). Automated MAD and MIR structure solution. *Acta Crystallogr. Sect. D*, **55**, 849–861.
38. Terwilliger, T. C. (2000). Maximum-likelihood density modification. *Acta Crystallogr. Sect. D*, **56**, 965–972.
39. Terwilliger, T. C. (2003). Automated main-chain model building by template matching and iterative fragment extension. *Acta Crystallogr. Sect. D*, **59**, 38–44.
40. Cowtan, K. (2006). The Buccaneer software for automated model building: 1. Tracing protein chains. *Acta Crystallogr. Sect. D*, **62**, 1002–1011.
41. Murshudov, G. N., Vagin, A. A., Lebedev, A., Wilson, K. S. & Dodson, E. J. (1999). Efficient anisotropic refinement of macromolecular structures using FFT4. *Acta Crystallogr. Sect. D*, **55**, 247–255.
42. Storoni, L. C., McCoy, A. J. & Read, R. J. (2004). Likelihood-enhanced fast rotation functions. *Acta Crystallogr. Sect. D*, **60**, 432–438.